Journal of Molecular Spectroscopy 332 (2017) 38–44

Contents lists available at ScienceDirect

Journal of Molecular Spectroscopy

journal homepage: www.elsevier.com/locate/jms

Gas-phase complexes of Ni^{2+} and Ca^{2+} with deprotonated histidylhistidine (HisHis): A model case for polyhistidyl-metal binding motifs

Katrin Peckelsen [a], Jonathan Martens [b], Giel Berden [b], Jos Oomens [b,c], Robert C. Dunbar [d], Anthony J.H.M. Meijer [e,*], Mathias Schäfer [a,*]

[a] Department of Chemistry, Institute of Organic Chemistry, University of Cologne, Greinstraße 4, 50939 Cologne, Germany
[b] Radboud University, Institute for Molecules and Materials, FELIX Laboratory, Toernooiveld 7c, 6525ED Nijmegen, The Netherlands
[c] University of Amsterdam, Science Park 904, 1098XH Amsterdam, The Netherlands
[d] Chemistry Department, Case Western Reserve University, Cleveland, OH 44106, USA
[e] Department of Chemistry, University of Sheffield, Sheffield S3 7HF, UK

ARTICLE INFO

Article history:
Received 15 August 2016
In revised form 4 October 2016
Accepted 13 October 2016
Available online 14 October 2016

Keywords:
Infrared multiple photon dissociation
IRMPD spectroscopy
Nickel and calcium-histidylhistidine complexes
Density functional theory computations
Iminolate and charge solvation binding patterns

ABSTRACT

In the complex formed between the calcium cation (Ca^{2+}) and a deprotonated HisHis dipeptide, the complex adopts a charge solvation (CS) structure. Ca^{2+}, a weak binding main group metal cation, interacts with the oxygens of the peptide carbonyl moiety and the deprotonated C-terminus. In contrast, the much stronger binding Ni^{2+} cation deprotonates the peptide nitrogen and induces an iminolate (Im) ligand structure in the $[Ni(HisHis-H)]^+$ complex ion. The combination of infrared multiple-photon dissociation (IRMPD) spectroscopy and quantum chemistry evidence these two representative binding motifs. The iminolate coordination pattern identified and characterized in the $[Ni(HisHis-H)]^+$ complex serves as a model case for nickel complexes of poly-histidyl-domains and is thereby also of interest to better understand the fundamentals of immobilized metal ion affinity chromatography as well as of Ni co-factor chemistry in enzymology.

1. Introduction

Proteins with consecutive histidine residues are frequently found in nature *e.g.* in bacterial chaperones, prion proteins, intrinsically unstructured proteins [1,2], snake venoms and also in nuclear speckles of human cells [3]. The biological function of such His-rich proteins (Hrp) in the latter cell compartments is completely unknown. However, it is certain that His residues in Hrps are excellent binding sites for transition metals, like Cu^{2+} and Ni^{2+}, making Hrps often responsible for metal ion transport and homeostasis [3,4]. The strong metal affinity of histidine is also the origin for the elevated sensitivity of histidine residues towards metal-catalyzed oxidation, which leads to the formation of 2-oxo-His residues [5,6]. Furthermore, Ni^{2+} serves as an enzymatic co-factor by inducing Hrps to adopt defined metal-complex conformations, which are apparently important for the function of these extensively investigated Hrps [1–4]. Nevertheless, many aspects of transition metal binding to Hrps are yet not understood. To study the fundamental coordination motifs of polyhistidine-metal complexes, we selected two exemplary cationic complexes of calcium and nickel with a deprotonated histidylhistidine ligand as simplified model analytes [3,4].

Nickel in the oxidation state II has an electronic configuration of $[Ar]3d^8 4s^0$ with outer d electrons making it a typical 'late' transition metal with a relatively small ion radius (0.69 Å). In fact, Ni^{2+} cations exhibit a high chelation binding strength to Lewis basic ligand atoms, preferentially to nitrogen, if available [7–9]. Strong interactions of Ni^{2+} with histidine residues are therefore typical if the side-chain imidazole nitrogen is not protonated (pK_a imidazole 6.9), which is the case at physiological pH (7.4) [3,10], explaining the relevance of Hrps for specific protein purification and fractionation by immobilized metal ion affinity chromatography (IMAC) [3,11]. For IMAC, Hrps or proteins intentionally decorated with hexa-His tags (H_6) can be selectively addressed as they bind strongly to immobilized nickel cations that are fixed to a stationary solid support [12]. Elution of the Hrps from the column is simply

* Corresponding authors.
E-mail addresses: a.meijer@sheffield.ac.uk (A.J.H.M. Meijer), mathias.schaefer@uni-koeln.de (M. Schäfer).

http://dx.doi.org/10.1016/j.jms.2016.10.008
0022-2852/

achieved by lowering the pH to values of about 4.0, inducing protonation of the imidazole nitrogen-metal binding site and the release of the Ni^{2+} from the protein-metal complex, highlighting the pH-dependence of the Ni^{2+} polyhistidyl-complex stability [11].

Besides the important role of the imidazole side chain moiety of His for transition metal binding, Lewis acidic metal cations also coordinate to peptide backbone nitrogens as experimental evidence by X-ray crystallography [13], NMR spectroscopy [10], ion mobility spectrometry [14] and IRMPD spectroscopy [8,15,16] proves. In fact, divalent metal ions like Cu^{2+} and Ni^{2+} induce the deprotonation of peptide backbone amide nitrogens and leave the acidic C-terminus in the condensed phase untouched. The dissociation of a backbone amide nitrogen proton facilitates an anionic binding site in an iminolate peptide ligand for the complexation of a metal cation. The proton is easily transferred to the polar condensed phase, whereas in the gas phase the proton rearranges and an iminol ligand structure is formed [15]. The remarkable iminol gas-phase binding pattern introduced and investigated by Dunbar and co-workers is a direct consequence of the effective desolvation, which leaves metal-peptide complexes in the vacuum of an MS-instrument without a solvation shell, making the elimination of the proton to the surrounding vacuum energetically impossible and eventually enforcing the formation of the iminol tautomer [7,8,13,15–17]. Here, we chose to study singly-charged complex ions of divalent metal cations with a deprotonated histidylhistidine ligand with the aim to mimic solution phase conditions as closely as possible.

On the other hand, we want to probe whether the nature of the metal cation can trigger a different binding motif in the HisHis ligand. Therefore, the analogous calcium complex $[Ca(HisHis-H)]^+$ was also included in this investigation as a characteristic comparison. Calcium was chosen because this alkaline-earth metal cation is much larger (0.99 Å) than Ni^{2+}, more polarizable, and therefore binds substantially weaker to peptide ligands. Moreover, peptide-Ca^{2+} complexes typically feature a C-terminally deprotonated peptide ligand [8,15,18].

To analyze the structure of the selected pair of complex ions, infrared multiple-photon dissociation (IRMPD) spectroscopy experiments were conducted on a modified 3D-quadrupole ion trap (QIT) mass spectrometer equipped with an electrospray (ESI) ionization source [19]. Wavelength tunable infrared light from the FELIX free electron laser was used for IRMPD as has been described elsewhere [19]. The singly charged metal-HisHis complexes $[M(HisHis-H)]^+$ with M = Ni^{2+} and Ca^{2+} were synthesized according to a standard protocol [20] and the respective precursor ions were trapped, mass selected and irradiated in the QIT. The extremely low density of ions in any tandem MS precludes measurement of gas-phase IR spectra in transmission and therefore IRMPD spectra are acquired by monitoring the extent of precursor ion depletion and product ion formation as the frequency of the IR radiation used for activation is tuned between 5 and 20 μm. Hence, IRMPD spectroscopy is a true action spectroscopy method [21–23]. The IRMPD spectra are compared to calculated IR spectra of candidate structures identified by density functional theory (DFT: B3LYP-GD3BJ functional/ cc-pVTZ basis set) [24–30], making a reliable assignment of individual isomers, tautomers and conformers possible. Although straightforward, this approach is limited to analytes with a manageable number of IR active chromophores to avoid spectral congestion. We considered these important prerequisites for successful IRMPD spectroscopy and selected the relatively short histidylhistidine ligand, which serves as a simplified model for His-rich protein domains and also for the hexa-His tags used in IMAC, as they allow one to study the fundamentals of the Ni(II)-protein coordination through the His side-chain imidazoles as well as the potential involvement of peptide bond nitrogens.

2. Experiment

2.1. Materials: dipeptide HisHis synthesis

The HisHis-dipeptide ligand was synthesized by André Reinhardt MSc in the working group of Professor Ines Neundorf, University Cologne. The synthesis of HisHis was performed on solid support according to the following standard protocol. 4-Benzyloxybenzyl alcohol polystyrene (Wang resin) beads (resin loading: 1.1 mmol/g; mesh size: 200–400 mesh; 0.024 mmol scale) were used in an automated peptide synthesizer Syro I from MultiSynTech. The peptide coupling was performed as double coupling steps using DIC (N,N-diisopropyl-carbodiimide) and Oxyma pure (Novabiochem and IRIS Biotech). Peptides were cleaved from the resin using triflouroacetic acid (TFA)/triisopropylsilane (TIS) and water (95:2.5:2.5 v/v/v) for 3 h and precipitated in ice-cold *n*-hexane/diethyl ether (1:3, v/v). Peptides were washed five times with 10 mL ice-cold *n*-hexane/diethyl ether (1:3, v/v) and lyophilized from water with *tert*-butyl alcohol (Fluka) (3:1, v/v).

2.2. Mass spectrometry

The $[M(HisHis-H)]^+$ complexes of (a) Ni^{2+} and (b) Ca^{2+} were freshly prepared for this study [20] and characterized by positive ion mode electrospray ionization (+ESI) mass spectrometry (MS). Both complexes were prepared in H_2O/ethanol and this solution was diluted with methanol to a concentration of about 10^{-5} M for (+)ESI-MS. All (+)ESI-MS and MS^2 experiments, as well as accurate mass measurements, were conducted on a ThermoFisher LTQ-Orbitrap XL instrument (ThermoFisher, Bremen Germany, see Supporting Information Table S1). Accurate ion masses were determined in the orbitrap analyzer with a resolution of 30,000 FWHM with external calibration ($\Delta m < 3$ ppm) or with addition of internal standards ($\Delta m < 2$ ppm, see Supporting Information Table S2). Typical (+)ESI-MS conditions were: Flow rate 5 μL min^{-1}; Capillary Voltage 3.20 kV; Sheath gas 4.99 [arb. units]; Aux gas 2.00 [arb. units].

2.3. Infrared multiphoton-dissociation spectroscopy

A modified quadrupole ion trap mass spectrometer (Bruker, Amazon Speed ETD) was used for the IRMPD spectroscopy experiments and has been described in detail elsewhere [19]. Tunable radiation for the photo-dissociation experiments was generated by the Free Electron Laser for Infrared eXperiments (FELIX) in the 500–1800 cm^{-1} range. Pulse energies were approximately 20–50 mJ per macropulse for the FEL. The full width at half maximum (fwhm) bandwidth of the FEL is approximately 0.5% of the central wavelength. Precursor ions for IRMPD experiments ($[Ni(HisHis-H)]^+$ at m/z 349 and $[Ca(HisHis-H)]^+$ at m/z 331) were formed by (+)ESI from solutions of 0.5 μM in CH_3OH:H_2O at a flow rate of 120 μL h^{-1} for each of the respective analytes. All ions were irradiated for 1 s, corresponding to interaction with 2 macropulses of FELIX. The IRMPD spectra were recorded by monitoring the intensity of the product ions (see Supporting Information Table S1) and the depletion of the respective precursor ion as a function of IR frequency. The IRMPD yield was determined from the precursor intensity (I_P) and the intensity of the fragment ions ($\Sigma I_{\text{fragment ions}}$) after laser irradiation at each frequency [19,22,23].

$$\text{IRMPD Yield} = \Sigma I_{\text{fragment ions}}/(I_P + \Sigma I_{\text{fragment ions}}) \quad (1)$$

Yields are linearly corrected for frequency-dependent variations in laser power.

3. Theory

Density functional theory (DFT) calculations were performed using Gaussian09, version D.01 [24]. Gaussian was compiled with Gaussian-supplied versions of BLAS and ATLAS [25,26]. The B3LYP functional was used throughout with the GD3-BJ correction to account for dispersion interactions, whereby it is noted that in this case this correction did not change results significantly compared to the bare B3LYP functional [27,28]. The cc-pVTZ basis set was used throughout with the ultrafine setting for the integrals [29,30]. This computational procedure was found to give good correlation with experiment in previous work [31]. All the calculations performed on these systems were done *in vacuo*. Frequencies were scaled by 0.97 to account for anharmonicity and convoluted with a Gaussian lineshape function with a FWHM of 12 cm^{-1} to facilitate comparison with experiment [21–23]. Energy differences quoted throughout the paper are based on Gibbs free energies (298 K, 1 bar). In all cases, the lowest-energy Ni(II) complexes were found to have a triplet spin state, whereas for Ca(II) complexes a singlet spin state was consistently lowest in energy. Ion structures identified by theory are denoted in a straightforward way as illustrated in Scheme 1. The initial two letters indicate the tautomer type of the ligand, being either iminolate (Im) with a deprotonated amide nitrogen (Scheme 1 structure a), charge solvated (CS) with a deprotonated C-terminus (Scheme 1 structure b) or iminol (II) with an iminol motif of the peptide linkage and a deprotonated C-terminus (Scheme 1 structure c). The following capital letters in brackets refer to the heteroatom coordination sites of the metal ion in the complex, *e.g.* Im[NNNNO]. In the $Im[NNNN]_{OH}$ case, the OH index denotes the additional hydrogen bond present in this complex ion.

4. Results

The IRMPD-spectra of the $[M(HisHis-H)]^+$ complex molecular ions with $M = Ni^{2+}$ (a) and $M = Ca^{2+}$ (b) are presented in Fig. 1. A direct comparison of the two spectra identifies the absorption bands that are most relevant for both complex ions. These vibrational modes are found at 580 cm^{-1}, 1080 cm^{-1} and at 1430 cm^{-1} and can be attributed to vibrational modes of the histidine imidazole side chain heterocycle. In addition to spectral similarities, Fig. 1 also reveals at least two clearly distinctive wavenumber regions, which are also important for the analysis. Firstly, major differences are found in the 1100–1400 cm^{-1} wavenumber range in which C-OH stretching and CO-H bending modes are resonant. The absence of any absorption in this region in the IRMPD-spectrum of the $[Ca(HisHis-H)]^+$ complex molecular ion (Fig. 1b) clearly indicates the deprotonation of the C-terminus, whereas the strong bands found in that region in the spectrum of the $[Ni(HisHis-H)]^+$ complex ion point towards a different deprotonation site in the HisHis ligand in the nickel complex. Secondly, the IRMPD-spectrum of the $[Ca(HisHis-H)]^+$ complex (Fig. 1b) exhibits two bands near 760 and 820 cm^{-1} with medium intensity, which are not observed in the spectrum of the analogous nickel complex ion (Fig. 1a). These absorptions correspond to vibrations of the amide proton and the carboxylate

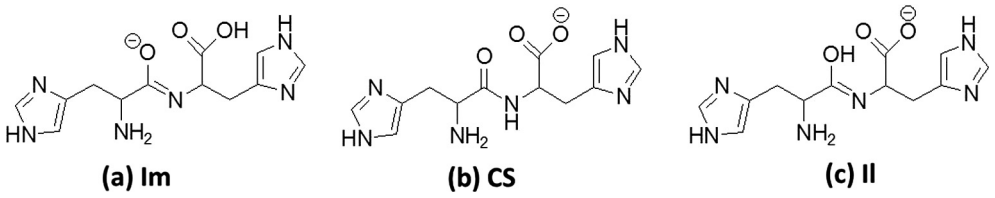

Scheme 1. Notation of the deprotonated HisHis ligand tautomers: (a) iminolate (Im), (b) charge solvated (CS) and (c) iminol (II).

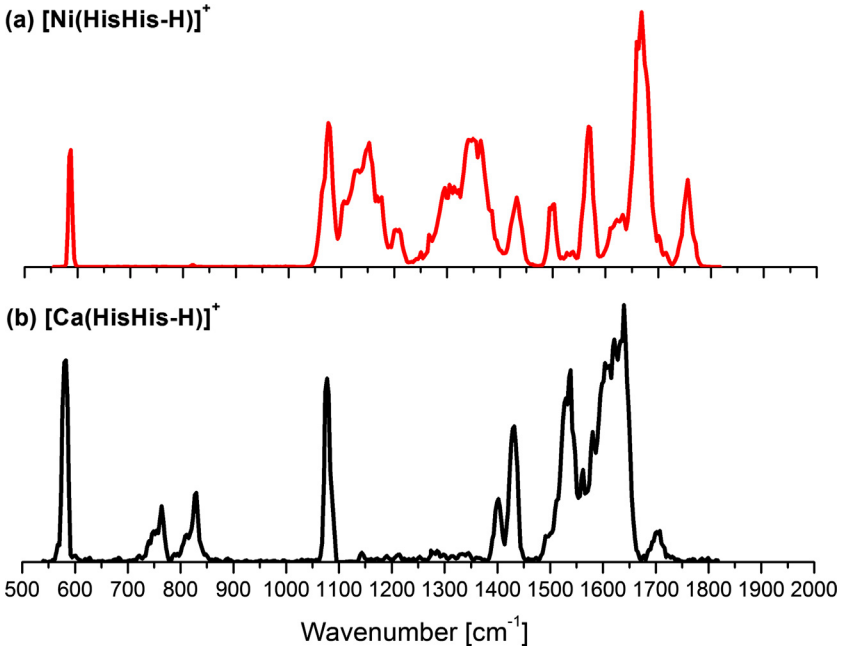

Fig. 1. Comparison of IRMPD spectra of (a) the $[Ni(HisHis-H)]^+$ complex and (b) the $[Ca(HisHis-H)]^+$ complex molecular ion.

moiety ($RCOO^-$ scissoring mode of the deprotonated C-terminus) in the $[Ca(HisHis-H)]^+$ case (see Tables S3 and S4 in the SI for band origins and assignments).

In line with this qualitative evaluation of the IRMPD-spectra are the ground state structures of the two complex ions that were identified by theory as Fig. 2 illustrates. The structure of the $[Ni(HisHis-H)]^+$ complex (Fig. 2, structure a) exhibits a pyramidal coordination sphere around the Ni^{2+} ion, where the ligand adopts the iminolate tautomeric form Im[NNNNO] [8]. Interestingly, for this ion a triplet spin state is lower in energy than any singlet spin state. Coordination occurs through the [NNNNO] heteroatoms in this structure, corresponding to the deprotonated amide nitrogen, the N-terminal amine nitrogen, the His-side-chain imidazole nitrogens and the C-terminal carbonyl oxygen. The ion shown in Fig. 2b is the ground state structure of the $[Ca(HisHis-H)]^+$ complex with typical CS binding pattern. In this CS[NNOO] ion, the Ca^{2+} ion interacts predominantly with the His-side-chain imidazole nitrogens, the amide carbonyl oxygen and the deprotonated C-terminal carboxylate group [8,15,18].

In Fig. 3 the computed IR spectra of three competitive iminolate conformers (Gibbs energies within 3.4 kJ mol^{-1} of each other) of $[Ni(HisHis-H)]^+$ are compared to the experimental spectrum of the molecular ion at m/z 349 (black trace). The structures presented in panels a–c have the characteristic iminolate (Im) binding motif in common and are similarly stable according to the DFT calculations (see SI for details). The structure $Im[NNNN]_{O-H}$ (3.4 kJ mol^{-1}) has an additional hydrogen bond interaction between the peptide bond iminolate oxygen and the C-terminal carboxyl proton giving rise to a diagnostic band near 1400 cm^{-1}, where the CO-H bending and the C-OH stretching modes are resonant. Both the Im[NNNN] structure (Panel b) and the Im[NNNNO] structure (Panel c) exhibit this band having combined C-OH stretching / CO-H bending character shifted to the red near 1150 cm^{-1}. In the Im[NNNN] structure (Panel b) where the Ni^{2+} ion interacts primarily with four nitrogens, the asymmetric carbonyl stretching modes $\nu_{C=O}$ of the peptide bond and of the C-terminus are found around 1660 and 1750 cm^{-1}, respectively. These two modes are characteristically shifted in the IR spectra of the other two conformers providing diagnostic insights into the nature of these individual complex structures. For the Im[NNNNO] structure (Panel c), the C-terminal carbonyl stretching band is strongly red shifted due to the interaction with the Lewis

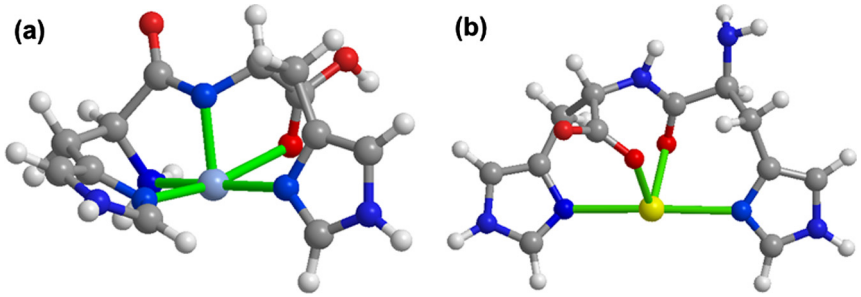

Fig. 2. Most stable $[M(HisHis-H)]^+$ complex structures of (a) Ni^{2+} and (b) Ca^{2+} proposed by theory. (a) Im[NNNNO] ion structure of the $[Ni(HisHis-H)]^+$ complex and (b) CS[NNOO] ion structure of $[Ca(HisHis-H)]^+$. Coordinative metal-ligand interactions are highlighted with green lines; color coding for atoms: C gray, H white, O red, N blue, Ni^{2+} gray-blue, Ca^{2+} yellow. (For interpretation of the references to color in this figure legend, the reader is referred to the web version of this article.)

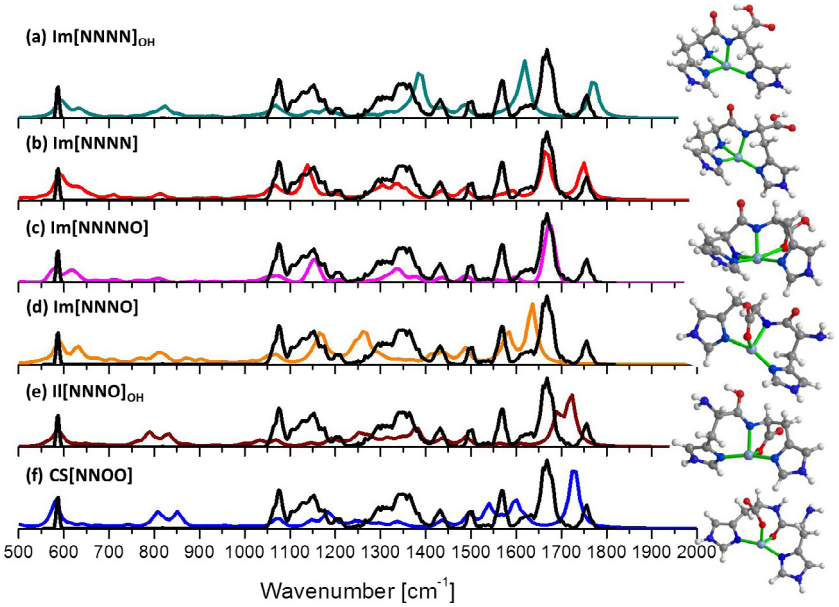

Fig. 3. Calculated IR spectra of three low-energy iminolate conformers of $[Ni(HisHis-H)]^+$ (a) $Im[NNNN]_{OH}$ (3.4 kJ mol^{-1}); (b) Im[NNNN] (3.1 kJ mol^{-1}); (c) Im[NNNNO] (0.0 kJ mol^{-1}) and an energetically disfavored analogue in panel (d) Im[NNNO] (49.7 kJ mol^{-1}). Also included in this comparison is an iminol structure $II[NNNO]_{OH}$ (25.6 kJ mol^{-1}) in panel (e) as well as a charge solvation structure CS[NNOO] (f) (analogous to the respective $[Ca(HisHis-H)]^+$ structure; 25.6 kJ mol^{-1}; see Fig. 4). All computed spectra are compared to the IRMPD spectrum of the molecular ion of $[Ni(HisHis-H)]^+$ at m/z 349 (black trace) [8,15,18]. All band origins of computed isomers of $[Ni(HisHis-H)]^+$ are presented in Table S3 in the Supporting Information.

acidic Ni^{2+} ion and merges with the peptide carbonyl stretch in a strong band at 1670 cm^{-1}. On the other hand, the computed spectrum of the Im[NNNN]$_{O\text{-}H}$ structure (Panel a) exhibits a red-shifted peptide carbonyl stretching mode $\nu_{C=O}$ (1620 cm^{-1}), which matches the shoulder in the IRMPD-spectrum of $[Ni(HisHis\text{-}H)]^+$ ion, and a blue-shifted C-terminus $\nu_{C=O}$ band (1770 cm^{-1}), both reflecting the influence of the hydrogen bond interaction on the position of the carbonyl vibrations. However, the strong absorption band at 1570 cm^{-1} is missing in the computed IR spectra of the iminolate ion structures discussed above. The band at 1570 cm^{-1} could be explained by a scissoring mode of the free and non-coordinated N-terminal amine group of another Im[NNNO] ion structure of the $[Ni(HisHis\text{-}H)]^+$ complex (see Panel d, Fig. 1), although this isomer is clearly disfavored by energy (49.7 kJ mol^{-1}).

In total, the IRMPD-spectrum of $[Ni(HisHis\text{-}H)]^+$ shows many significant features which are in good agreement with the computed linear IR-spectra of a set of iso-energetic iminolate ion structures identified by DFT computations, suggestive of their simultaneous presence (see also Fig. S1, SI for a comparison of a Boltzmann weighted composite spectrum vs the IRMPD-spectrum of $[Ni(HisHis\text{-}H)]^+$).

Another unique complex structure of the $[Ni(HisHis\text{-}H)]^+$ ion is identified by theory in the extended stability range but the IR-spectrum of the Il[NNNO]$_{OH}$ structure is substantially differing from the IRMPD-spectrum (Fig. 3e). This structure exhibits a deprotonated C-terminus and an iminol motif of the peptide backbone, where the amide nitrogen interacts with the nickel cation (compare Scheme 1, structure c) [16]. Additionally, this Il [NNNO]$_{OH}$ structure (25.6 kJ mol^{-1}) possesses a hydrogen bond interaction between the free amino nitrogen and the iminol OH. Combined modes of the N-terminal amine N-H and the respective O-H···N hydrogen bond are found near 790 and 830 cm^{-1} in the computed IR-spectrum of the Il[NNNO]$_{OH}$ ion structure. However, these two bands are absent in the IRMPD spectrum in Fig. 3e. We also note a weak band in the computed spectrum of the iminolate ion structure Im[NNNN]$_{OH}$ found around 820 cm^{-1} in Panel 3a, which comes from the twisting mode of the hydrogen bond COO-H···O between the carboxylic hydrogen and the iminolate oxygen. Similarly, a weak band at 820 cm^{-1} is found in Panel 3d in the IR-spectrum of the Im[NNNO] structure corresponding to out of plane modes of the imidazole hydrogens. While absorptions in this wavenumber range correspond to combined vibrations of the carboxylate moiety ($RCOO^-$ scissoring mode of the deprotonated C-terminus) and the amide proton in CS[NNOO] charge solvation complex structures (compare Panel 3f, Fig. 1 and Fig. 4), the examples above show that the absence of these bands in the IRMPD spectrum of the nickel complex is less significant than initially believed (see discussion of Fig. 1).

Finally, an energetically disfavored charge solvation structure CS[NNOO] of the nickel complex (25.6 kJ mol^{-1}) is also compared with the IRMPD-spectrum of $[Ni(HisHis\text{-}H)]^+$ in Panel f. Especially the mismatch of the computed carbonyl bands as well as the absence of the C-OH stretching and CO-H bending vibrations makes the presence of this alternative structure unlikely.

In Fig. 4, the IRMPD spectrum (black trace) of $[Ca(HisHis\text{-}H)]^+$ is compared with the computed IR-spectrum of the energetically favored charge solvation structure CS[NNOO] (0.0 kJ mol^{-1}). The overlay presentation in panel a documents a good match in the significant regions of the spectrum (700–900 cm^{-1} and 1000–1400 cm^{-1}) as pointed out above. More importantly, the major band at 1538 cm^{-1}, which corresponds to the amide N-H bending mode, engaged in a hydrogen-bond interaction with the N-terminal amine nitrogen, and the strong absorption at 1608 cm^{-1} (amide carbonyl stretching mode) match the absorptions in the IRMPD-spectrum very well. However, the computed C-terminal carbonyl stretching vibration that is expected to appear at 1720 cm^{-1} is actually found red shifted at 1702 cm^{-1} in the IRMPD-spectrum. Moreover, the measured IRMPD-yield and the band intensity predicted by theory differ substantially, which may be due to a reduced laser intensity in this frequency range in combination with a strongly non-linear power dependence, and/or due to a missed conformation in the computations [32,33].

The comparison of the two computed IR-spectra in panels a and b of Fig. 4 reveals remarkable band positions of the C-terminal carbonyl stretch vibration in the two isomeric ion structures. In the CS

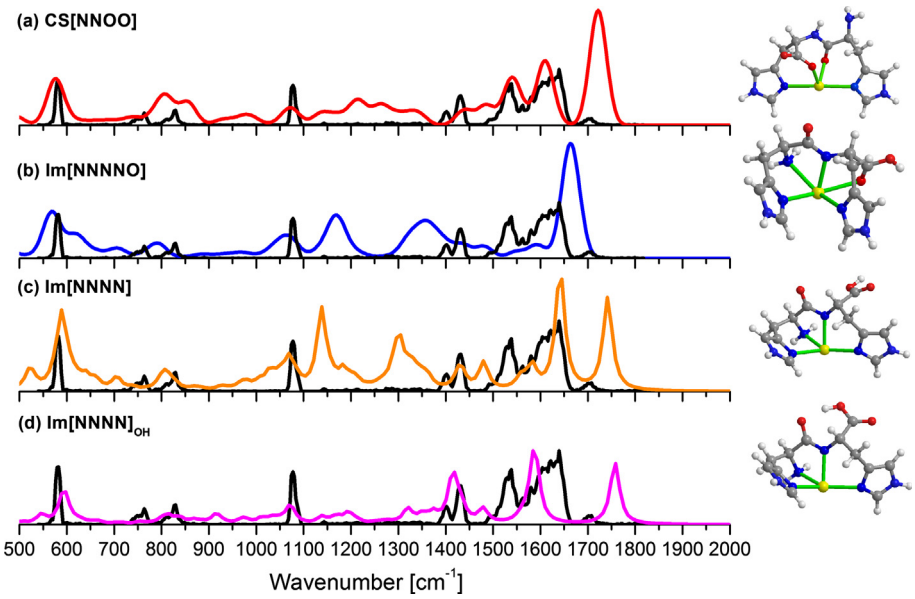

Fig. 4. The IRMPD-spectrum of $[Ca(HisHis\text{-}H)]^+$ at *m/z* 331 (black trace) is compared to computed IR-spectra of ion structures identified by theory [16,18]. (a) IR-spectrum of the charge solvation structure CS[NNOO] (0.0 kJ mol^{-1}). (b) IR-spectrum of iminolate isomer Im[NNNNO] (22.0 kJ mol^{-1}). (c) IR-spectrum of iminolate isomer Im[NNNN] (58.9 kJ mol^{-1}). (d) IR-spectrum of iminolate isomer Im[NNNN]$_{OH}$ (53.6 kJ mol^{-1}). All band origins of the computed isomers of $[Ca(HisHis\text{-}H)]^+$ are presented in Table S4 in the Supporting information.

[NNOO] ion structure (Panel a), this mode of the deprotonated C-terminal carboxylate functionality is substantially blue-shifted relative to the analogous mode of the free carboxylic acid moiety RCOOH in the Im[NNNNO] structure of $[Ca(HisHis-H)]^+$ that appears at about 1670 cm^{-1} in panel b. The observed blue-shifted carbonyl vibration indicates a substantial strengthening of the C=O bond of the carboxylate moiety in the CS[NNOO] structure, which is the result of the coordination to the Lewis acidic Ca^{2+} metal cation. This phenomenon was already described and observed in IRMPD spectra of metal cationized histidine $[M(His-H)]^+$ complexes of zinc and cadmium [24].

In Fig. 4b–d, the iminolate ion structures are presented with their computed IR-spectra for evaluation. The mismatch of the computed IR-spectrum of the energetically disfavored iminolate isomer Im[NNNNO] (22.0 kJ mol^{-1}) with the IRMPD-spectrum of $[Ca(HisHis-H)]^+$ especially in the region from 1000 to 1400 cm^{-1} of the diagnostic C-OH and CO-H modes leads us to exclude this complex structure [8,15,18]. The theoretical IR-spectrum of the iminolate complex Im[NNNNO] (58.9 kJ mol^{-1}), which is substantially unstable in the calcium case, is also found to be unlikely for similar reasons (Fig. 4c). This assumption is further supported by the inspection of the C-terminal carbonyl stretching mode at 1740 cm^{-1}, which is found to be substantially blue shifted compared to the respective mode in the IRMPD-spectrum. Finally, the IR-spectrum of the $Im[NNNN]_{OH}$ ion structure (Panel d), which is also disfavored for energetic reasons (53.6 kJ mol^{-1}), is found to be an unlikely candidate due to the clear disagreement of its carbonyl modes in the 1500–1800 cm^{-1} region with the IRMPD-spectrum. Detailed information on all ion structures of the $[Ca(HisHis-H)]^+$ complex ion is provided in the Supporting Information and in Table S4.

5. Conclusions

The data set presented above provides initial spectroscopic evidence that the nature of the metal cation governs the binding motif in $[M(HisHis-H)]^+$ complex ions with a deprotonated histidylhistidine ligand.

The combination of IRMPD spectroscopy and quantum-chemical calculations identifies an iminolate structure in $[Ni(HisHis-H)]^+$ and a charge solvation (CS) structure in the $[Ca(HisHis-H)]^+$ complex, which also documents the detailed information on the coordination sphere of the metal and the complex geometry that is provided by this approach [8,15,18]. In $[Ni(HisHis-H)]^+$ the strongly binding nickel(II) cation prefers to deprotonate the peptide-bond nitrogen over the C-terminus and induces tautomerization of the amide bond resulting in an iminolate (Im) ion structure of the HisHis-ligand. This remarkable behavior highlights the pronounced preference of the nickel(II) cation for stabilization by peptidic Lewis-basic nitrogen atoms over oxygen atoms. This experimental finding qualitatively explains why complex ions of nickel(II) with a deprotonated histidine amino acid molecule are not sufficiently stable for (+)ESI-MS characterization [32], whereas complex ions with two histidine amino acids *i.e.* $[Ni(His)(His-H)]^+$ are. The latter complexes are currently being investigated computationally and experimentally by IRMPD spectroscopy [34].

The iminolate binding pattern is shown to be optimal for metal ion coordination in the $[Ni(HisHis-H)]^+$ complex and it can serve as a model example to better understand the fundamentals of IMAC, as well as the nature of Hrp-Ni^{2+} interactions co-factor chemistry. However, to clarify the binding mode of nickel(II) cations to *e.g.* His-tags with 6 consecutive histidine residues as used in IMAC, further investigations will be necessary.

In this regard it will be important to also study whether the amide backbone interaction of the metal cation remains relevant even with longer and more flexible peptidic ligands with more than 2 imidazole side-chain moieties, *e.g.* in $[Ni(HisHisHis-H)]^+$ complex ions. At present, the binding pattern in polyHis-protein domains to nickel(II) ions remains unclear and the relation of thermodynamic stability of respective metal complexes with the number of histidine residues in the coordinating fragment is not fully understood [3,4].

Acknowledgements

The authors gratefully acknowledge the FELIX staff, particularly Dr. B. Redlich and Dr. A.F.G. van der Meer, as well as Professor Ines Neundorf and M.Sc. André Reinhardt, University Cologne, Institute of Biochemistry for the skilful preparation of HisHis. The research leading to these results has received funding from the European Community's Seventh Framework Program (FP7/2007-2013) under grant agreement no. 312284. This work is in part supported by a research program of FOM, which is financially supported by NWO.

Appendix A. Supplementary material

Supplementary data associated with this article can be found, in the online version, at http://dx.doi.org/10.1016/j.jms.2016.10.008.

References

[1] M. Miraula, S. Ciurli, B. Zambelli, Intrinsic disorder and metal binding in UreG proteins from Archae hyperthermophiles: GTPase enzymes involved in the activation of Ni(II) dependent urease, J. Biol. Inorg. Chem. 20 (2015) 739–755.
[2] P. Faller, C. Hureau, G. La Penna, Metal ions and intrinsically disordered proteins and peptides: from Cu/Zn amyloid-β to general principles, Acc. Chem. Res. 47 (2014) 2252–2259.
[3] M. Rowinska-Zyrek, D. Witkowska, S. Potocki, M. Remelli, H. Kozlowski, His-rich sequences – is plagiarism from nature a good idea?, New J Chem. 37 (2013) 58–70.
[4] D. Witkowska, R. Politano, M. Rowinska-Zyrek, R. Guerrini, M. Remelli, H. Kozlowski, The coordination of Ni(II) and Cu(II) ions to the polyhistidyl motif of Hpn protein: is it as strong as we think?, Chem Eur. J. 18 (2012) 11088–11099.
[5] K. Inoue, C. Garner, B.L. Ackermann, T. Oe, I.A. Blair, Liquid chromatography/tandem mass spectrometry characterization of oxidized amyloid beta peptides as potential biomarkers of Alzheimer's disease, Rapid Commun. Mass Spectrom. 20 (2006) 911–918.
[6] A.K.Y. Lam, C.A. Hutton, R.A.J. O'Hair, Role of 2-oxo and 2-thioxo modifications on the proton affinity of histidine and fragmentation reactions of protonated histidine, Rapid Commun. Mass Spectrom. 24 (2010) 2591–2604.
[7] R.C. Dunbar, N.C. Polfer, G. Berden, J. Oomens, Metal ion binding to peptides: oxygen or nitrogen sites?, Int J. Mass Spectrom. 330–332 (2012) 71–77.
[8] R.C. Dunbar, G. Berden, J. Oomens, How does a small peptide choose how to bind a metal ion? IRMPD and computational survey of CS versus Iminol binding preferences, Int. J. Mass Spectrom. 354–355 (2013) 356–364.
[9] R.C. Dunbar, Spectroscopy of metal-ion complexes with peptide-related ligands, Top. Curr. Chem. 364 (2015) 183–224.
[10] R. De Ricco, S. Potocki, H. Kozlowski, D. Valensin, NMR investigations of metal interactions with unstructured soluble protein domains, Coor. Chem. Rev. 269 (2014) 1–12.
[11] R. Chi Fai Cheung, J. Ho Wong, T. Bun Ng, Immobilized metal ion affinity chromatography: a review on its applications, Appl. Microbiol. Biotechnol. 96 (2012) 1411–1420.
[12] A. Battistoni, F. Pacello, A.P. Mazzetti, C. Capo, J.S. Kroll, P.R. Langford, A. Sansone, G. Donnarumma, P. Valenti, G. Rotilio, A histidine-rich metal binding domain at the N terminus of Cu, Zn-superoxide dismutases from pathogenic bacteria, J. Biol. Chem. 276 (2001) 30315–30325.
[13] D.P. Fairlie, T.C. Woon, W.A. Wickramasinghe, A.C. Willis, Amide-imino tautomerism: effect of metalation, Inorg. Chem. 33 (1994) 6425–6428.
[14] T. Wyttenbach, D. Liu, M.T. Bowers, Interactions of the hormone oxytocin with divalent metal ions, J. Am. Chem. Soc. 130 (2008) 5993–6000.
[15] R.C. Dunbar, J.D. Steill, N.C. Polfer, G. Berden, J. Oomens, Peptide bond tautomerization induced by divalent metal ions: characterization of the iminol configuration, Angew. Chem. Int. Ed. 51 (2012) 4591–4593.
[16] R.C. Dunbar, G. Berden, J.K. Martens, J. Oomens, Divalent metal-ion complexes with dipeptide ligands having Phe and His side-chain anchors: effects of sequence, metal ion, and anchor, J. Phys. Chem. A 119 (2015) 9901–9909.
[17] I. Sóvágó, K. Ösz, Metal ion selectivity of oligopeptides, Dalton Trans. (2006) 3841–3854.
[18] R.C. Dunbar, J. Oomens, G. Berden, J. Kai-Chi Lau, U.H. Verkerk, A.C. Hopkinson, K.W. Michael Siu, Metal ion complexes with HisGly: comparison with PhePhe and PheGly, J. Phys. Chem. A 117 (2013) 5335–5343.

[19] J. Martens, J. Grzetic, G. Berden, J. Oomens, Structural identification of electron transfer dissociation products in mass spectrometry using infrared ion spectroscopy, Nat. Commun. 7 (2016) 11754.
[20] S.-Y. Ke, C.-C. Wang, G.-H. Lee, Y.-C. Chuang, K.-L. Lu, Highly thermal-stable supramolecular assembly of a hydrogen-bonded mononuclear nickel(II) histidine compound, J. Chin. Chem. Soc. 60 (2013) 807–812.
[21] W.H. Wing, G.A. Ruff, J.W.E. Lamb, J. Spezeski, Observation of the infrared spectrum of the hydrogen molecular ion HD^+, Phys. Rev. Lett. 36 (1976) 1488–1491.
[22] N.C. Polfer, J. Oomens, Vibrational spectroscopy of bare and solvated ionic complexes of biological relevance, Mass Spectrom. Rev. 28 (2009) 468–494.
[23] N.C. Polfer, Infrared multiple photon dissociation spectroscopy of trapped ions, Chem. Soc. Rev. 40 (2011) 2211–2221.
[24] M.J. Frisch, G.W. Trucks, H.B. Schlegel, G.E. Scuseria, M.A. Robb, J.R. Cheeseman, G. Scalmani, V. Barone, B. Mennucci, G.A. Petersson, H. Nakatsuji, M. Caricato, X. Li, H.P. Hratchian, A.F. Izmaylov, J. Bloino, G. Zheng, J.L. Sonnenberg, M. Hada, M. Ehara, K. Toyota, R. Fukuda, J. Hasegawa, M. Ishida, T. Nakajima, Y. Honda, O. Kitao, H. Nakai, T. Vreven, J.A. Montgomery Jr., J.E. Peralta, F. Ogliaro, M. Bearpark, J.J. Heyd, E. Brothers, K.N. Kudin, V.N. Staroverov, R. Kobayashi, J. Normand, K. Raghavachari, A. Rendell, J.C. Burant, S.S. Iyengar, J. Tomasi, M. Cossi, N. Rega, J.M. Millam, M. Klene, J.E. Knox, J.B. Cross, V. Bakken, C. Adamo, J. Jaramillo, R. Gomperts, R.E. Stratmann, O. Yazyev, A.J. Austin, R. Cammi, C. Pomelli, J.W. Ochterski, R.L. Martin, K. Morokuma, V.G. Zakrzewski, G.A. Voth, P. Salvador, J.J. Dannenberg, S. Dapprich, A.D. Daniels, Ö. Farkas, J.B. Foresman, J.V. Ortiz, J. Cioslowski, D.J. Fox, Gaussian 09, Revision D.01, Gaussian Inc., Wallingford, CT, 2009.
[25] R. Clint Whaley, A. Petitet, J.J. Dongarra, Automated empirical optimizations of software and the ATLAS project, Parallel Comput. 27 (2001) 3–35.
[26] R.C. Whaley, A. Petitet, Minimizing development and maintenance costs in supporting persistently optimized BLAS, Softw. Pract. Exp. 35 (2005) 101–121.
[27] A.D. Becke, Density-functional thermochemistry. III. The role of exact exchange, J. Chem. Phys. 98 (1993) 5648–5652.
[28] S. Grimme, S. Ehrlich, L. Goerigk, Effect of the damping function in dispersion corrected density functional theory, J. Comput. Chem. 32 (2011) 1456–1465.
[29] T.H. Dunning Jr., Gaussian basis sets for use in correlated molecular calculations. I. The atoms boron through neon and hydrogen, J. Chem. Phys. 90 (1989) 1007–1023.
[30] N.B. Balabanov, K.A. Peterson, Systematically convergent basis sets for transition metals. I. All-electron correlation consistent basis sets for the 3d elements Sc–Zn, J. Chem. Phys. 123 (2005) 064107.
[31] M. Schäfer, K. Peckelsen, M. Paul, J. Martens, J. Oomens, G. Berden, A. Berkessel, A.J.H.M. Meijer, Hydrogen tunnelling at room temperature evidenced by infrared ion spectroscopy, J. Am. Chem. Soc. (2016) (submitted for publication).
[32] T.E. Hofstetter, C. Howder, G. Berden, J. Oomens, P.B. Armentrout, Structural elucidation of biological and toxicological complexes: investigation of monomeric and dimeric complexes of histidine with multiply charged transition metal (Zn and Cd) cations using IR action spectroscopy, J. Phys. Chem. B 115 (2011) 12648–12661.
[33] F. Dreiocker, J. Oomens, A.J.H.M. Meijer, B.T. Pickup, R.F.W. Jackson, M. Schäfer, Structure elucidation of dimethylformamide solvated alkylzinc cations in the gas phase, J. Org. Chem. 75 (2010) 1203–1213.
[34] K. Peckelsen, J. Martens, G. Berden, J. Oomens, A.J.H.M. Meijer, M. Schäfer, Int. J. Mass Spectrom. (2016) (in preparation).